Available online at www.sciencedirect.com

ScienceDirect

Ceramics International 40 (2014) 173–180

CERAMICS INTERNATIONAL

www.elsevier.com/locate/ceramint

Enhancing the performance of front-illuminated dye-sensitized solar cells with highly [001] oriented, single-crystal-like TiO_2 nanotube arrays

Zuobao Yang[a,*], Zhongquan Ma[a,*], Dengyu Pan[b], Dongsheng Chen[a], Fei Xu[a], Shumin Chen[a]

[a]SHU-SolarE R&D Lab, Department of Physics, Shanghai University, Shanghai 200444, PR China
[b]Institute of Nanochemistry and Nanobiology, Shanghai University, Shanghai 200444, PR China

Received 5 May 2013; received in revised form 28 May 2013; accepted 30 May 2013
Available online 5 June 2013

Abstract

Highly ordered, vertically aligned TiO_2 nanotube arrays (TNAs) have been prepared by a modified two-step anodic oxidation. The second as-prepared TNAs show smoother surface, fewer cracks and more uniform nanotubes on large scale compared with the first as-grown one. With different content of water in anodizing electrolyte, highly oriented TNAs and arbitrarily oriented TNAs were obtained. The narrow dominant peak of (004) of XRD shows that the TNAs are highly crystallized. Moreover, the interplanar distance of 0.237 nm, the marked angle in fast Fourier transform of 68.3° and the diffraction fringe on the margin of tube wall by high-resolution transmission electron microscopy demonstrate that the highly oriented TNAs are single-crystal-like anatase in nature with highly exposed (001) facets which grow along the [001] direction. The TNAs have been detached and transferred to Fluorine-doped Tin Oxide substrate successfully as transparent photo-anodes for assembling dye-sensitized solar cells. Under front-side illumination, DSSCs based on highly [001] oriented TNAs show a remarkable enhancement of 29% in power conversion efficiency and faster electron transport compared to that of arbitrarily oriented TNAs. The influence of the thickness on the performance of the DSSCs based on highly [001] oriented TNAs is investigated and the best power conversion efficiency of 5.73% is achieved.

Keywords: Single-crystal-like; TiO_2 nanotube arrays; Front-illuminated; Dye-sensitized solar cells

1. Introduction

Dye-sensitized solar cells (DSSCs) have attracted great interest in scientific and industrial fields due to their low cost, impressive power conversion efficiency (PCE) and easy fabrication as compared to conventional p–n junction solar cells during the past two decades [1–5]. DSSCs also show a relatively better performance under diffuse light and higher temperature conditions than other solar cells [6]. Typically, DSSCs are composed of a layer of TiO_2 nanocrystals, a counter electrode, a dye-load sensitizer and an electrolyte. Recently, using such structure, the highest PCE exceeding 12% has been achieved [7]. However, further improvement in performance of such DSSC would be limited owing to tremendous grain boundaries and disordered pore structure in the interconnecting nanoparticles that lead to slow electron transport [8,9] during the charge transport process [10–12]. Accordingly, one dimensional (1D) nanostructures such as nanotubes [13–16], nanowires [17,18] and nanorods [19–21], which are expected to remarkably enhance photo-generated electron transport, have been introduced to prepare the photo-anodes of the DSSCs. In this regard, anodic TiO_2 nanotubes have been widely used because of its superior dye adsorption both in inner and outer of tube wall as well as adjustable highly functional geometry to others since it was first reported [22]. Apart from the better charge collection and slow recombination of the TiO_2 nanotube arrays (TNAs), excellent intrinsic light scattering to harvest sunlight toward longer wavelength [23] is beneficial to TNA-based DSSCs and thus leads to improve the performance to some degree [24–26].

*Corresponding authors. Tel.: +86 21 66136912; fax: +86 21 66136907.
E-mail addresses: hokepoly@hotmail.com (Z. Yang), zqma@shu.edu.cn (Z. Ma).

0272-8842/$ - see front matter © 2013 Elsevier Ltd and Techna Group S.r.l. All rights reserved.
http://dx.doi.org/10.1016/j.ceramint.2013.05.119

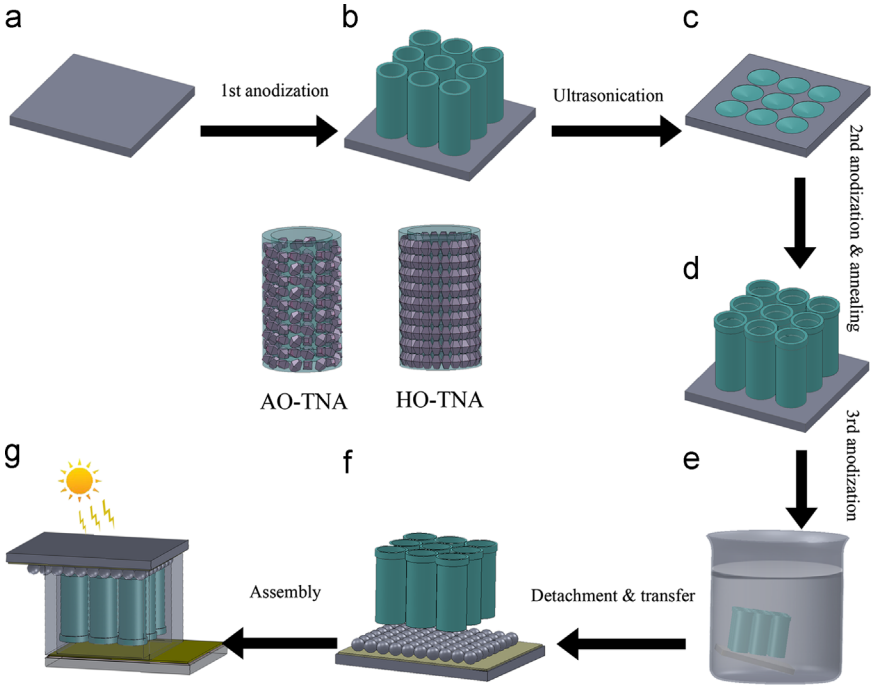

Scheme 1. Scheme for preparation of highly [001] oriented TNAs (a–d), detachment and transfer of TNAs (e and f) and assembly of front-illuminated DSSCs (g).

Even though the TNA-based DSSCs are expected to take most of the advantages above mentioned, traditional DSSCs based on anodized TNAs still encounter issues lowering the efficiency. First, DSSCs based on TNAs starting from an opaque Ti substrate require back-side illumination which incident light is only possible from the opposite side and it will suffer a degradation of the performance due to undesirable light absorption of the iodine electrolyte and partially light reflection of the Pt counter electrode under such illumination [27]. To address this issue, transparent photo-anodes by anodizing sputtered Ti thin film [28,29] on and transferring anodized TNAs [30] to the Fluorine-doped Tin Oxide (FTO), have been employed to fabricate front-illuminated DSSCs. With regard to the sputtering route, except for the high cost and complexity of the process, the limited thickness of TNAs is another problem. Secondly, crystallized anatase TNAs usually exhibit dominant (101) facet or random stacking of (101) and (001) facets which grain is arbitrarily oriented in the one-dimensional TNA. Compared with TiO_2 nanoparticle-based DSSCs, although charge recombination of such TNAs was considerable suppressed, but for electron transport, there was no substantial improvement [13] owing to arbitrary grain orientations and less reactive (101) facets. On the other hand, since single crystal anatase TiO_2 with large percent reactive (001) facets reported by Yang and co-works [31], many efforts have been attempted to develop new routes on dominant (001) anatase TiO_2 crystals in powder or film forms and its applications [32,33]. Experimental investigations have shown that the (001) facets of anatase TiO_2 exhibited more reactive compared to (101) facets in application of photovoltaic devices and photocatalysis [34,35] as well due to the unique surface structure characteristics. However, in comparison with the TiO_2 nanoparticles or powders, it is still a challenge to prepare such TNAs with much more reactive (001) facets which will induce a highly [001] oriented, vertically aligned growth and thus facilitate electron transport. Moreover, detachment and transfer such highly [001] oriented TNAs for front-illuminated dye-sensitized solar cells, which has never been attempted, it to be more attractive.

Herein, in the present work, highly ordered TNAs were prepared in a suitable electrolyte with a modified two-step electrochemical anodic oxidation. These TNAs were detached from the Ti substrate by a facile electrochemical route and transferred to the FTO glass substrate. Using a thin layer of TiO_2 nanoparticles as adhesion layer, the detached TNAs were firmly attached to the substrate and accordingly, the DSSCs based on highly [001] oriented, single-crystal-like TNAs (HO-TNA) show a significant improvement (~29%) in PCE compared to that of based on arbitrarily oriented TNAs (AO-TNA). The electrochemical impedance spectroscopy was employed to investigate the electrons transportation on the nanotubes. Additionally, the influence in the thickness of the HO-TNA on the performance of the DSSCs was explored.

2. Experimental section

2.1. Preparation of highly ordered TNAs

The highly ordered TNAs were prepared by a two-step potentiostaic anodic oxidation in a two-electrode cell with a graphite sheet as the counter electrode at room temperature. The scheme for preparation of highly oriented TNAs was illustrated in Scheme 1a–f. Prior to first anodic oxidation, Ti foils (Schemes 1a, 0.25 mm in thickness, 99.7% in purity, Sigma-Aldrich) were polished in a mixed solution containing hydrofluoric acid (HF), nitride acid (HNO_3) and DI water (HF:HNO_3:DI = 1:4:5, v/v).

It was then degreased ultrasonically in acetone, ethanol and deionized (DI) water, respectively, and anodized for 2 h at 50 V DC bias in a mixed ethylene glycol solution containing 0.4 wt% NH_4F and a small amount of DI water. In this work, 2% and 4% in volume ratio of DI water were investigated. Afterwards, the as-prepared TNAs (Scheme 1b) were removed by sonication for several minutes in DI water leaving behind dimple-like footprints substrate (Scheme 1c). The second-step anodization was carried out in the same electrolyte for different time intervals to produce highly ordered TNAs with different thickness.

2.2. Detachment and transfer of TNAs

The as-prepared amorphous TNAs were crystallized into anatase phase at 450 °C for 2 h in air with a heating rate of 1.5 °C min^{-1}. After another anodization under the same condition for 10 min and then immersing into the H_2O_2 solution (33%) for 60 min (Scheme 1e), the anatase TNA membrane (Scheme 1d) was detached from the Ti substrate. Followed by rinsing and drying, the self-standing TNA membrane was cut into the sized of 5 mm × 5 mm for transfer. To transfer the self-standing TNAs to FTO substrate, 1 g of polyethylene glycol (PEG) coated TiO_2 nanoparticles (NP) which was prepared by a hydrothermal route [36], was uniformly dispersed in 5 mL DI water and then previous spin-coated onto FTO as a adhesion layer. Thereafter, the free-standing TNAs were carefully transferred to the TiO_2 NP-coated FTO substrate (Fig.1f). The transplanted TNAs were firmly adhered to the FTO substrate after annealing at 450 °C for 30 min at a heating rate of 1.5 °C min^{-1}.

2.3. Fabrication and measurement of the front-illuminated DSSCs

After cooling to ~80 °C, the TNA-FTO photo-anodes were immersed into anhydrous ethanol solution containing N719 dyes (0.3 mM, Solaronix) for 24 h at room temperature. Pt counter

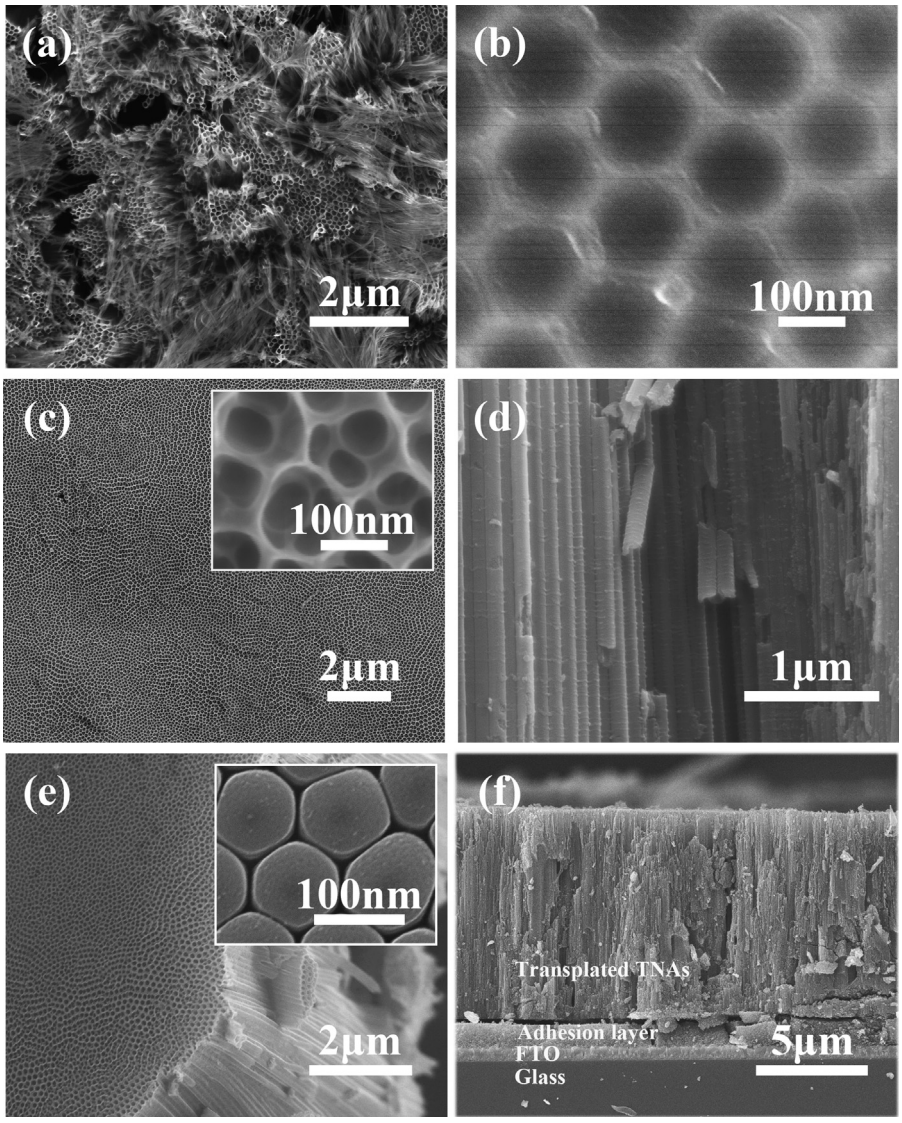

Fig. 1. FESEM images for (a) top view of TNAs after the first anodic oxidation, (b) Ti substrate after removing the first as-prepared TNAs, (c–e) TNAs after the second anodic oxidation: (c) top view, inset shows the magnitude top morphology; (d) three-dimensional view from top side; (e) three-dimensional view from bottom side, inset shows the bottom of the nanotubes and (f) cross-sectional view of the transplanted TNAs on FTO.

electrodes were prepared by dropping 5 mM H_2PtCl_6 isopropanol solution on apertured FTO glass, followed by heating at 390 °C for 30 min. After rinsing with ethanol and drying in air, the dye-loaded TNA-FTO films were assembled with the Pt/FTO electrode using a 60-μm-thick hot-melt sealed film as spacer (DHS-SN1760, Heptachroma, Dalian, China) and the structure of the devices is illustrated in Scheme 1g. The active area of the devices is approximately 0.25 cm^2. Finally, the redox electrolyte (acetonitrile solution of DMPII/LiI/I_2/TBP/GuSCN, DHS-E23, Heptachroma, Dalian, China) was injected into the cell through the aperture of the counter electrode. The photovoltaic performance of the DSSCs were measured using a computer-controlled keithly-2400 source meter under illumination intensity of 100 mW cm^{-2} at room temperature with a standard solar simulator. Electrochemical impedance spectroscopy (EIS) measurement was carried out with an electrochemical workstation (CHI660D, CH instruments, Shanghai, China).

2.4. Characterization

The morphology and crystallinity of the TNAs were characterized by field emission scanning electron microscopy (FESEM, S4800, Hitachi, Japan) and X-ray powder diffraction (XRD, D/Max-2500V, Rigaku, Japan), respectively. The microstructures were further investigated with a high-resolution transmission electron microscope (HRTEM, JEM-2010F, JEOL, Japan). The amount of adsorbed N719 dyes was estimated by measuring the desorbed dyes from TNAs with ultraviolet-visible (UV–vis) absorption spectroscopy with a spectrophotometer (U3010, Hitachi, Japan).

3. Results and discussion

Irregular top morphology of TNAs such as bundles, cracks and debris will strongly affect electron transport, and consequently result in a detrimental performance of DSSCs. To focus on investigating the influence of the highly [001] oriented TNAs on the performance of DSSCs, these undesirable factors should be exclude. To this end, a second anodic oxidation was performed to produce the uniform TNAs. Fig. 1a shows the FESEM image for TNAs prepared after first anodic oxidation in the mixed ethylene glycol solution. It was observed that some surface debris, cracks and some "nano-grass" covered on the top surface of the resulting TNAs, which not only inhibited infiltration of dye molecules and electrolyte throughout the TNAs but also increased chance of recombination by introducing disorder defects, and consequently affected photo-generated electrons transport as well. Ultrasonic vibration was, in general, used to remove these unwanted deposits introduced during the first anodic oxidation. However, the surface flatness of the TNAs is hard to control and, sometimes, the TNAs may be partly delaminated during ultrasonication. Accordingly, we removed the first as-prepared TNAs and anodized the resulting dimple-like Ti substrate (Scheme 1c and Fig. 1b). Compared with the first anodized TNAs, the second as-prepared TNAs exhibited smoother surface (Fig. 1c), fewer cracks, uniform tubular structure and were vertical oriented (Fig. 1e) to the membrane surface. Specifically, a top mesporous layer (inset in Fig. 1c) formed over the TiO_2 nanotubes may act as a combined layer to buffer the stress during growth and subsequent annealing processes, thereby induce smoother surface. The average outer diameter of the mesporous layer and the inner diameter of the nanotube beneath the mesporous layer were approximately 118 nm and 80 nm, respectively. After anodizing for another additional 10 min under the same conditions and immersing into H_2O_2 solution (Scheme 1e), these TNAs were peeled off completely from the Ti substrate, which was probably due to destruction of the unstable amorphous new thin layer grown during the third anodic oxidation between the crystallized TNAs and Ti substrate. Nevertheless, the detached TNAs membranes themselves are difficult to adhesive to the FTO substrate directly. To facilitate this process, the PEG-coated TiO_2 NP paste was spin-coated on the FTO glass as an adhesion layer, followed by transplanting the self-standing TNAs on its top (Scheme 1f) with a gentle pressure. The resulting samples were then annealed at 450 °C for 30 min in air to ensure excellent contact between TNAs and adhesion NP layer. Fig. 1f demonstrated that the self-standing TNAs remained intact and tightly attached to the FTO glass through the TiO_2 NP adhesion layer after sintering. Four layers from top to bottom were clearly observed: the transplanted TNAs, the TiO_2 NP adhesion layer, FTO and glass. The corresponding thicknesses, determined from the cross-section view of FESEM image (Fig. 1f), were approximate 9.5 μm, 0.9 μm, 0.5 μm and 2.2 mm, respectively.

Recent studies [37,38] have shown that (001) and (101) facets of anatase TiO_2 exhibit different adsorption of water which may affect the growth rate in different orientation of the crystals [39]. Here we prepare the TNAs using ethylene glycol containing 2 vol % and 4 vol% of water. To exclude the effects of the thickness of the TiO_2 membrane, the TNAs with nearly equal thickness, corresponding to 9.5 μm and 9.7 μm, were prepared by controlling the anodized reaction time to be 1.0 h and 1.5 h, respectively. These TNAs were crystallized, detached from the Ti foil and transferred to FTO substrate. The crystal structure of the resulting samples was characterized with XRD as shown in Fig. 2. The XRD patterns of both samples exhibited prominent peaks at (101), (004) and (200) which were assigned to anatse TiO_2 (JCPDS no.12-2172). Similar results of XRD patterns for both TNAs before detachment were observed (Fig. S1, ESI). Furthermore, no rutile-phase was observed except for some diffraction peaks resulting from FTO substrate. However, with the different amount of water in the electrolyte, the resulting samples showed different dominant peaks. For 4 vol% of water, the as-grown sample exhibited main peaks of (101) with relative intensity of (004) and (200) (Fig. 2a) which revealed arbitrarily crystallographic orientation in TNAs. Such arbitrarily oriented TNA was designated as AO-TNA and accordingly the AO-TNA with the thickness of 9.7 μm was designated as AO-TNA-9.7 hereafter. Nevertheless, when content of the water in electrolyte was turn to be 2 vol%, it was found that a dominant peaks of (004) with high intensity and narrow Full Width at Half Maximum (FWHM) was observed (Fig. 2b). The intensity ratio of the (004) diffraction

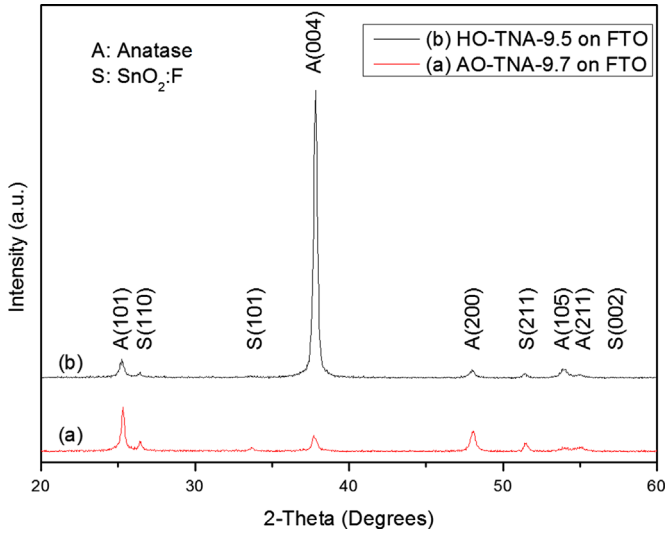

Fig. 2. XRD patterns of the as-annealed HO-TNA-9.5 and AO-TNA-9.7 on FTO substrate.

peak to that of (200) peak was about 32 which suggested that the resulting sample was highly crystallized and exhibited highly preferential oriented growth along the [001] direction. These highly [001] oriented TNA was designated as HO-TNA and accordingly such TNA with the thickness of 9.5 μm was designated as HO-TNA-9.5 hereafter. The HO-TNA with much more reactive (001) facets [31] are expected to significantly improve electrons transport and promising in application of photocatalysis and photovoltaic devices. The results above mentioned implied that the content of the water in electrolyte affected the crystallographic growth orientation but so far, the mechanism is not clear and it needs to be explored.

More detail structure of the HO-TNA was examined by HRTEM. Fig. 3 shows the TEM images of the nanotubes which scraped off from HO-TNA-9.5 samples. Typically, the tubular structure was clearly observed by low magnification TEM (Fig. 3a) and the average thickness of the tube-wall and the inner diameter of the nanotube were approximately 15 nm and 80 nm, respectively, which is consistent with the SEM images as shown in Fig. 1. The spacing of the lattice fringes on the tube-wall, determined from high-resolution TEM images (Fig. 3b), was estimated to be 0.237 nm corresponding to interplanar spacing of the anatase (001), which are in accordance with XRD patterns. Furthermore, the electron diffraction fringe of the fast Fourier transform (FFT, inset of Fig. 3b) from the selected area, which was marked with square mark in Fig. 3b on tube wall, did not show the polycrystalline ring patterns but single-crystal-like spot patterns. The marked angle (inset of Fig. 3b) was 68.3° which was identical to the theoretical value for the angle between (001) and (101) facets in an anatase TiO_2 crystal [40]. Moreover, the diffraction fringe on the margin of the tube wall (Fig. 3b) indicated that the as-annealed HO-TNA-9.5 was single-crystal-like anatase in nature with high exposed (001) facets and grown along the [001] direction which facilitated the photo-generated electron transport. With such single-crystal-like anatase HO-TNA, the chance of the recombination for photo-generated electrons could be significantly reduced during transportation, and consequently, the larger diffusion length of the electron will be obtained on nanotube. Compared with AO-TNA, the thicker HO-TNA film which can absorb more dye molecules and effectively enhance the photoelectric performance is expected to apply in DSSCs as a photo-anode.

To evaluate the influence of crystallographic orientation on the performances of TNA-based DSSCs, we fabricated DSSCs with the HO-TNA-9.5 and AO-TNA-9.7. The DSSCs were assembled using N719 dyes as a sensitizer of the photo-anodes, the I^-/I_3^- redox couple as an electrolyte, and platinized FTO glass as a counter electrode, and the performances of the cells were measured using front-illumination mode under simulated AM 1.5 G sunlight (100 mW cm^{-2}). The current–voltage (J–V) characteristics of the representative samples were shown in Fig. 4, and typical performance parameters, such as open-circuit voltage (V_{oc}), short-circuit current density (J_{sc}), fill factor (FF), and power conversion efficiency (PCE) were summarized in Table 1. Different from the nearly equal open circuit voltage (V_{oc}) of both samples, which were 0.67 V for AO-TNA-9.7 and 0.65 V for HO-TNA-9.5, respectively, the significant improvement in short circuit density (J_{sc}) from 6.38 mA cm^{-2} to 8.24 mA cm^{-2} was obtained with the HO-TNA-9.5 compared to that of AO-TNA-9.7. Accordingly, the considerable improvement in PCE, which the PCE increase from 3.07% for AO-TNA-9.7 to 3.96% for HO-TNA-9.5, exhibited enhancement of 29% to that of AO-TNA-9.7. For the same type of photo-anodes and dye molecules, the amount of the dye adsorption is the key factor of influence on the current density of the DSSCs. The monolayer N719 dyes anchored on both two samples were desorbed in a 0.1 M NaOH solution composed of mixed solvent (DI:ethanol = 1:1, v/v) and the amount of N719 dye was estimated by measuring UV–vis absorption spectroscopy of the resultant solution. Dye adsorbance was determined to be 2.58×10^{-7} mol cm^{-2} and 2.64×10^{-7} mol cm^{-2} for AO-TNA-9.7 and HO-TNA-9.5, respectively. For the nearly equal thickness of the TNAs and identical dye molecules used in this work, the significant improvement in J_{sc} could not be explained by the slight difference of the dye adsorbance. It was probably attributed to the single-crystal-like nature and the high exposed reactive facet of anatase (001), which grew along to the tube wall and perpendicular to the substrate, and consequently, photo-generated electrons injected from the dye molecules under the incident light were effectively collected during transportation compared to that of AO-TNA.

To explore the interface and the electron transport properties of TNAs, electrochemical impedance spectroscopy (EIS) was characterized with an applied DC bias value of open circuit voltage in a perturbation alternative signal of 10 mV under illuminated of AM 1.5 G simulated solar light. The measuring frequency range was from 0.1 Hz to 10^5 Hz. Fig. 5 shows Nyquist plots obtained from the EIS characterization for each sample. The fitting data represented by continuous line show a good agreement with the measuring data represented by solid symbols according to corresponding equivalent circuit model [41,42] (inset of Fig. 5) with Zsimpwin software. In this work,

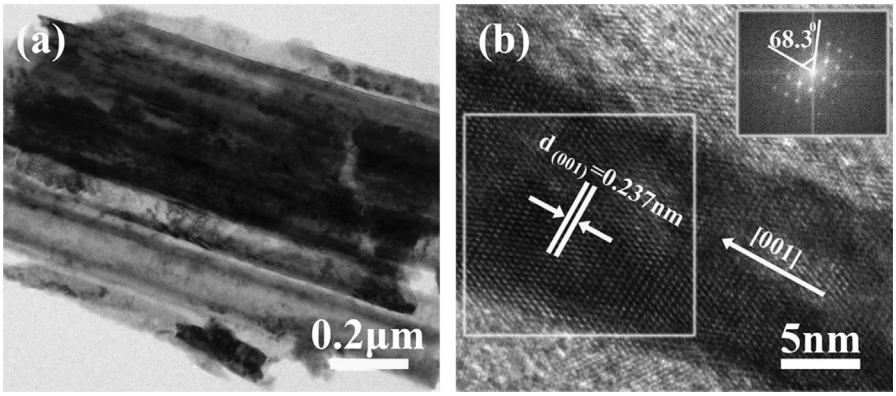

Fig. 3. TEM images of HO-TNA-9.5 with (a) low magnification and (b) high resolution. Inset is the fast Fourier transform (FFT) images obtained from the partial region that marked in Fig. 3b.

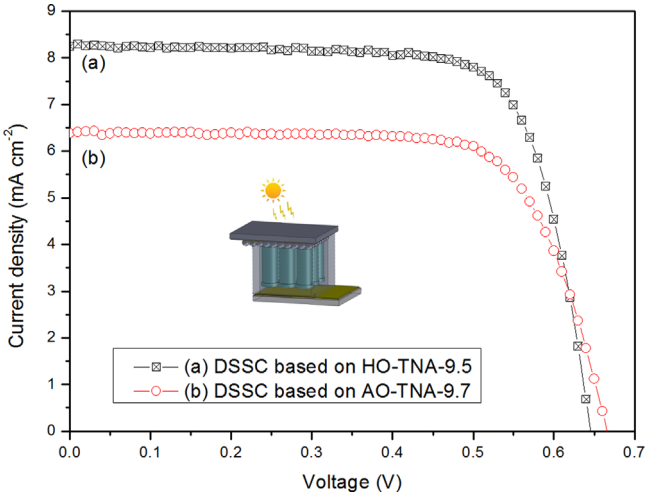

Fig. 4. Current–Voltage (J–V) characteristics of DSSCs based on HO-TNA-9.5 and AO-TNA-9.7.

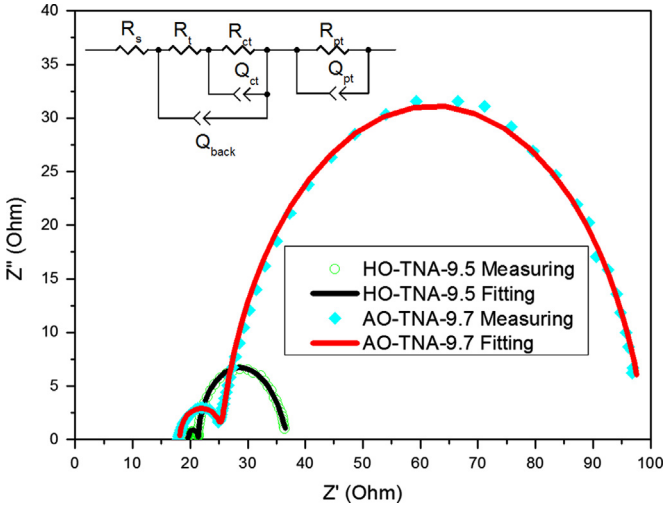

Fig. 5. Nyquist plots obtained from EIS for front-illuminated DSSCs based on AO-TNA-9.7 and HO-TNA-9.5. The symbols and continuous lines represent the measuring data and the fitting results, respectively. The insert shows the equivalent circuit which R_s is the series resistance of the FTO, R_t is the transport resistance of the electrons in TiO_2 nantube wall, R_{ct} is the charge-transfer resistance of the electrons in the TiO_2 nanotube and I_3^- in the electrolyte, the constant phase element Q_{ct} is the chemical capacitance of TiO_2 nanotube, Q_{back} is the additional capacitance of the exposed barrier layer of nanotube, R_{pt} and Q_{pt} represent the charge-transfer resistance and the interfacial capacitance at the platinized counter electrode and electrolyte interface respectively.

Table 1
The photovoltaic parameters of the DSSCs based on AO-TNA-9.7 and HO-TNA-9.5 and the corresponding extracted parameters from the EIS.

Sample	J_{sc} (mA cm^{-2})	V_{oc} (V)	FF (%)	PCE (%)	R_t (Ω)	R_{ct} (Ω)	Dye absorbance (10^{-7} mol cm^{-2})
AO-TNA-9.7	6.38	0.67	71.61	3.07	4.07	73.46	2.58
HO-TNA-9.5	8.24	0.65	73.85	3.96	0.19	15.65	2.64

we laid emphasis on the resistance parameters of EIS dependent on crystallographic orientation of the TNAs. As to the DSSCs based on AO-TNA and HO-TNA, the transport resistance R_t and charge-transfer resistance R_{ct} were taken into consideration because other parts was identical in the devices aside from the growth orientation of the TiO_2 crystal. The fitted data of transport resistance R_t and charge-transfer resistance R_{ct} extracted from the Nyquist plots of DSSCs based on HO-TNA-9.5 and AO-TNA-9.7 were summarized in Table 1. With the single-crystal-like HO-TNA-9.5, the transport resistance R_t about 0.19 Ω was one order of magnitude smaller than that (~4.07 Ω) of AO-TNA-9.7. It might be ascribed to vertical aligned [001] growth orientation of single-crystal-like HO-TNA thus leading to less scattering center from grain boundaries or traps on the crystallized nanotube. In contrast, the photo-injected electron on AO-TNA was apt to trapped due to a single sharp resonance arising from exciton-like trap states [43]. Accordingly, the larger electron diffusion coefficient [42] will be obtained for the single-crystal-like HO-TNA which lead to more photo-generated electrons surviving during transportation and improve the photocurrent. It is consistent with the larger current density for DSSC based on HO-TNA-9.5 which was characterized in photovoltaic performance in Fig. 4.

To investigate the influence of the thickness on the performance of the HO-TNA based DSSCs, more HO-TNAs with different thickness, corresponding to 12.3 μm, 15.1 μm, 18.8 μm, 20.2 μm and 25.1 μm, which were designated as HO-TNA-12.3, HO-TNA-15.1, HO-TNA-18.8, HO-TNA-20.2 and HO-TNA-25.1, respectively, were prepared and assembled into DSSCs. For comparison, the performance of the DSSC based on HO-TNA-9.5 was also put together. Fig. 6 showed the *J–V* characterization of the DSSCs under front-side illumination with the light intensity of 100 mW cm^{-2}. The short circuit current density (J_{sc}), open circuit voltage (V_{oc}), fill factor (FF) and power conversion efficiency (PCE) were summarized in Table 2. It could be observed that with the increase of thickness of the TNAs below 18.8 μm, which was obtained by anodic oxidation for 2 h, the J_{sc} exhibited a gradually increased from 8.24 mA cm^{-2} to 12.18 mA cm^{-2} while the V_{oc} was almost the same value. Consequently, the PCE exhibited continuous increase with the increase of the thickness and the best PCE of 5.73% was achieved with the thickness of 18.8 μm. Nevertheless, further increase in thickness of the TNAs, the PCE showed slightly decrease to 5.49% with thickness of 20.2 μm and 5.34% with thickness of 25.1 μm, respectively. The deteriorative trend of PCE with increasing thickness of the TNAs over 2 h for the reaction time of anodization was probably attributed to the destroy of surface geometry structure of the TNAs. With extended reaction time of anodization, the tube wall will be getting thinner and thinner and thus lead to cracks and surface debris on nanotubes. From the FESEM images (Fig. S2, ESI) of the TNAs with the thickness of 20.2 μm and 25.1 μm which were prepared for 2.5 h and 3.5 h anodization, respectively, the top combined layer were found to be etched away. Moreover, more cracks on nanotubes and nano-grass covered on the top of the nanotubes, which blocks the dye molecules and electrolyte infiltrating to the nanotube, was observed. To optimize photovoltaic performance of the DSSCs based on HO-TNAs, muti-step anodic oxidation, which reaction time of each step should be less than 2 h after the previous TNAs layer crystallizing in air, can be attempted to ensure the thicker and uniform TNAs and that will be investigated in the future.

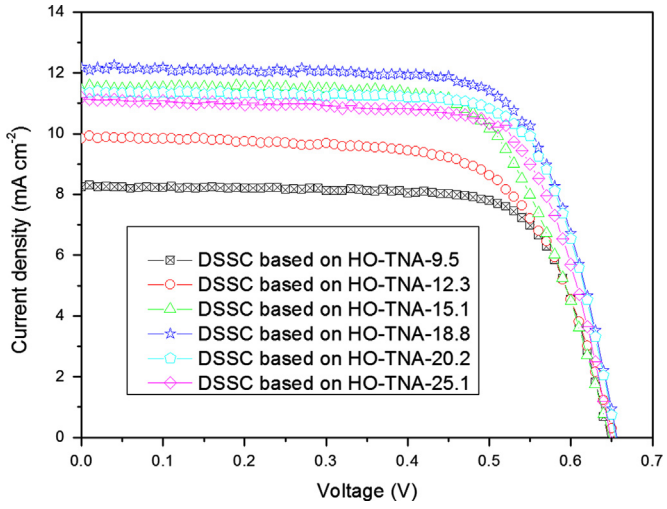

Fig. 6. Current–voltage (*J–V*) of the DSSCs with different thickness of HO-TNA.

Table 2
The parameters of the photovoltaic performance of the DSSCs with HO-TNAs.

Sample	Thickness (μm)	J_{sc} (mA cm^{-2})	V_{oc} (V)	*FF* (%)	*PCE* (%)
HO-TNA-9.5	9.5	8.24	0.65	73.85	3.96
HO-TNA-12.3	12.3	9.84	0.65	67.54	4.32
HO-TNA-15.1	15.1	11.44	0.65	68.86	5.12
HO-TNA-18.8	18.8	12.18	0.66	71.26	5.73
HO-TNA-20.2	20.2	11.35	0.65	74.53	5.49
HO-TNA-25.1	25.1	11.20	0.65	73.35	5.34

4. Conclusions

In summary, highly [001] oriented single-crystal-like TNAs have been prepared by a two-step electrochemical anodization. With a facile chemical route, the HO-TNAs were successfully detached from the Ti substrate and transferred to the TiO_2 nanoparticle-coated FTO. Under front-side illumination, the PCE of DSSC with HO-TNA shows an enhancement of 29% in comparison with that of AO-TNA. The results of the EIS reveal that DSSC with HO-TNA shows faster electron transport than that of AO-TNA. With regard to HO-TNA, the PCE of DSSCs increases gradually with increasing thickness of TNAs unless the top morphology of the nanotubes damaged due to the over-etching of tube wall. The best PCE has been achieved with 18.8 μm highly [001] oriented TNAs. The photovoltaic parameters give a J_{sc} of 12.18 mA cm^{-2}, a V_{oc} of 0.66 V and a FF of 71.26% corresponding to a PCE of 5.73% under front-illuminated mode of a simulated solar light (100 mW cm^{-2}).

Acknowledgments

This work was partly supported by the National Natural Science Foundation (Nos. 61274067, 60876045, 11174194, 11025526 and 91233102) of China, Shanghai Leading Basic Research Project (No. 09JC1405900), and R&D Foundation of SHU-SOENs PV Joint Lab (No. SS-E0700601) and Youth Science Fund Project of the Education Department of Jiangxi Province (No. GJJ10276). Part measurements were supported by Analysis and Testing Center of Shanghai University.

Appendix A. Supporting information

Supplementary data associated with this article can be found in the online version at http://dx.doi.org/10.1016/j.ceramint.2013.05.119.

References

[1] B. O'Regan, M. Gratzel, A low-cost, high-efficiency solar cell based on dye-sensitized colloidal TiO_2 films, Nature 353 (1991) 737–740.

[2] D.B. Kuang, S. Ito, B. Wenger, C. Klein, J.E. Moser, R. Humphry-Baker, S.M. Zakeeruddin, M. Gratzel, High molar extinction coefficient heteroleptic ruthenium complexes for thin film dye-sensitized solar cells, Journal of the American Chemical Society 128 (2006) 4146–4154.
[3] M. Gratzel, Photoelectrochemical cells, Nature 414 (2001) 338–344.
[4] M. Grätzel, Solar energy conversion by dye-sensitized photovoltaic cells, Inorganic Chemistry 44 (2005) 6841–6851.
[5] Y.J. Kim, M.H. Lee, H.J. Kim, G. Lim, Y.S. Choi, N.-G. Park, K. Kim, W.I. Lee, Formation of highly efficient dye-sensitized solar cells by hierarchical pore generation with nanoporous TiO_2 spheres, Advanced Materials 21 (2009) 3668–3673.
[6] A. Hagfeldt, G. Boschloo, L. Sun, L. Kloo, H. Pettersson, Dye-sensitized solar cells, Chemical Reviews 110 (2010) 6595–6663.
[7] A. Yella, H.W. Lee, H.N. Tsao, C. Yi, A.K. Chandiran, M. K. Nazeeruddin, E.W. Diau, C.Y. Yeh, S.M. Zakeeruddin, M. Gratzel, Porphyrin-sensitized solar cells with cobalt (II/III)-based redox electrolyte exceed 12 percent efficiency, Science 334 (2011) 629–634.
[8] J. Nelson, Continuous-time random-walk model of electron transport in nanocrystalline TiO_2 electrodes, Physical Review B 59 (1999) 15374–15380.
[9] J. Bisquert, Fractional diffusion in the multiple-trapping regime and revision of the equivalence with the continuous-time random walk, Physical Review Letters 91 (2003) 010602.
[10] J. Nelson, S.A. Haque, D.R. Klug, J.R. Durrant, Trap-limited recombination in dye-sensitized nanocrystalline metal oxide electrodes, Physical Review B 63 (2001) 205321.
[11] L. Dloczik, O. Ileperuma, I. Lauermann, L.M. Peter, E.A. Ponomarev, G. Redmond, N.J. Shaw, I. Uhlendorf, Dynamic response of dye-sensitized nanocrystalline solar cells: characterization by intensity-modulated photocurrent spectroscopy, Journal of Physical Chemistry B 101 (1997) 10281–10289.
[12] G. Schlichthörl, N.G. Park, A.J. Frank, Evaluation of the charge-collection efficiency of dye-sensitized nanocrystalline TiO_2 solar cells, Journal of Physical Chemistry B 103 (1999) 782–791.
[13] K. Zhu, N.R. Neale, A. Miedaner, A.J. Frank, Enhanced charge-collection efficiencies and light scattering in dye-sensitized solar cells using oriented TiO_2 nanotubes arrays, Nano Letters 7 (2006) 69–74.
[14] G.K. Mor, O.K. Varghese, M. Paulose, K. Shankar, C.A. Grimes, A review on highly ordered, vertically oriented TiO_2 nanotube arrays: fabrication, material properties, and solar energy applications, Solar Energy Materials and Solar Cells 90 (2006) 2011–2075.
[15] S. Lee, I.J. Park, D.H. Kim, W.M. Seong, D.W. Kim, G.S. Han, J.Y. Kim, H.S. Jung, K.S. Hong, Crystallographically preferred oriented TiO_2 nanotube arrays for efficient photovoltaic energy conversion, Energy and Environmental Science 5 (2012) 7989–7995.
[16] J.M. Macak, P. Schmuki, Anodic growth of self-organized anodic TiO_2 nanotubes in viscous electrolytes, Electrochimica Acta 52 (2006) 1258–1264.
[17] M. Adachi, Y. Murata, J. Takao, J. Jiu, M. Sakamoto, F. Wang, Highly efficient dye-sensitized solar cells with a titania thin-film electrode composed of a network structure of single-crystal-like TiO_2 nanowires made by the oriented attachment Mechanism, Journal of the American Chemical Society 126 (2004) 14943–14949.
[18] M. Law, L.E. Greene, J.C. Johnson, R. Saykally, P. Yang, Nanowire dye-sensitized solar cells, Nature Materials 4 (2005) 455–459.
[19] L. De Marco, M. Manca, R. Giannuzzi, F. Malara, G. Melcarne, G. Ciccarella, I. Zama, R. Cingolani, G. Gigli, Novel preparation method of TiO_2-nanorod-based photoelectrodes for dye-sensitized solar cells with improved light-harvesting efficiency, Journal of Physical Chemistry C 114 (2010) 4228–4236.
[20] M. Wang, J. Bai, F.Le Formal, S.-J. Moon, L. Cevey-Ha, R. Humphry-Baker, C. Grätzel, S.M. Zakeeruddin, M. Grätzel, Solid-state dye-sensitized solar cells using ordered TiO_2 nanorods on transparent conductive oxide as photoanodes, Journal of Physical Chemistry C 116 (2012) 3266–3273.
[21] Q. Huang, G. Zhou, L. Fang, L. Hu, Z.-S. Wang, TiO_2 nanorod arrays grown from a mixed acid medium for efficient dye-sensitized solar cells, Energy and Environmental Science 4 (2011) 2145–2151.
[22] D. Gong, C.A. Grimes, O.K. Varghese, W. Hu, R.S. Singh, Z. Chen E.C. Dickey, Titanium oxide nanotube arrays prepared by anodic oxidation, Journal of Materials Research 16 (2001) 3331–3334.
[23] L.-L. Li, C.-Y. Tsai, H.-P. Wu, C.-C. Chen, E.W.-G. Diau, Fabrication of long TiO_2 nanotube arrays in a short time using a hybrid anodic method for highly efficient dye-sensitized solar cells, Journal of Materials Chemistry 20 (2010) 2753–2758.
[24] J.M. Macák, H. Tsuchiya, A. Ghicov, P. Schmuki, Dye-sensitized anodic TiO_2 nanotubes, Electrochemistry Communications 7 (2005) 1133–1137.
[25] G.K. Mor, K. Shankar, M. Paulose, O.K. Varghese, C.A. Grimes, Use of highly-ordered TiO_2 nanotube arrays in dye-sensitized solar cells, Nano Letters 6 (2005) 215–218.
[26] K. Shankar, G.K. Mor, H.E. Prakasam, S. Yoriya, M. Paulose, O.K. Varghese, C.A. Grimes, Highly-ordered TiO_2 nanotube arrays upto 220 μm in length: use in water photoelectrolysis and dye-sensitized solar cells, Nanotechnology 18 (2007) 065707.
[27] D.-J. Yang, H. Park, S.-J. Cho, H.-G. Kim, W.-Y. Choi, TiO_2-nanotube-based dye-sensitized solar cells fabricated by an efficient anodic oxidation for high surface area, Journal of Physics and Chemistry of Solids 69 (2008) 1272–1275.
[28] C.-H. Chen, K.-C. Chen, J.-L. He, Transparent conducting oxide glass grown with TiO_2-nanotube array for dye-sensitized solar cell, Current Applied Physics 10 (2010) S176–S179.
[29] K. Lee, D. Kim, S. Berger, R. Kirchgeorg, P. Schmuki, Front side illuminated dye-sensitized solar cells using anodic TiO_2 mesoporous layers grown on FTO-glass, Electrochemistry Communications 22 (2012) 157–161.
[30] L.L. Li, Y.J. Chen, H.P. Wu, N.S. Wang, E.W.G. Diau, Detachment and transfer of ordered TiO_2 nanotube arrays for front-illuminated dye-sensitized solar cells, Energy and Environmental Science 4 (2011) 3420–3425.
[31] H.G. Yang, C.H. Sun, S.Z. Qiao, J. Zou, G. Liu, S.C. Smith, H.M. Cheng G.Q. Lu, Anatase TiO_2 single crystals with a large percentage of reactive facets, Nature 453 (2008) 638–641.
[32] H. Ariga, T. Taniike, H. Morikawa, M. Tada, B.K. Min, K. Watanabe, Y. Matsumoto, S. Ikeda, K. Saiki, Y. Iwasawa, Surface-mediated visible-light photo-oxidation on pure TiO_2 (001), Journal of the American Chemical Society 131 (2009) 14670–14672.
[33] X. Han, Q. Kuang, M. Jin, Z. Xie, L. Zheng, Synthesis of titania nanosheets with a high percentage of exposed (001) facets and related photocatalytic properties, Journal of the American Chemical Society 131 (2009) 3152–3153.
[34] L. Kavan, M. Grätzel, S.E. Gilbert, C. Klemenz, H.J. Scheel, Electrochemical and photoelectrochemical investigation of single-crystal anatase, Journal of the American Chemical Society 118 (1996) 6716–6723.
[35] L. Etgar, W. Zhang, S. Gabriel, S.G. Hickey, M.K. Nazeeruddin, A. Eychmüller, B. Liu, M. Grätzel, High efficiency quantum dot heterojunction solar cell using anatase (001) TiO_2 nanosheets, Advanced Materials 24 (2012) 2202–2206.
[36] X. Yan, D. Pan, Z. Li, Y. Liu, J. Zhang, G. Xu, M. Wu, Controllable synthesis and photocatalytic activities of water-soluble TiO_2 nanoparticles, Materials Letters 64 (2010) 1833–1835.
[37] M. Sumita, C. Hu, Y. Tateyama, Interface water on TiO_2 anatase (101) and (001) surfaces: first-principles study with TiO_2 slabs dipped in bulk water, Journal of Physical Chemistry C 114 (2010) 18529–18537.
[38] A. Vittadini, A. Selloni, F.P. Rotzinger, M. Grätzel, Structure and energetics of water adsorbed at TiO_2 anatase (101) and (001) surfaces, Physical Review Letters 81 (1998) 2954–2957.
[39] A. Selloni, Crystal growth:anatase shows its reactive side, Nature Materials 7 (2008) 613–615.
[40] U. Diebold, The surface science of titanium dioxide, Surface Science Reports 48 (2003) 53–229.
[41] F. Fabregat-Santiago, E.M. Barea, J. Bisquert, G.K. Mor, K. Shankar C.A. Grimes, High carrier density and capacitance in TiO_2 nanotube arrays induced by electrochemical doping, Journal of the American Chemical Society 130 (2008) 11312–11316.
[42] Q. Wang, S. Ito, M. Grätzel, F. Fabregat-Santiago, I. Mora-Seró, J. Bisquert, T. Bessho, H. Imai, Characteristics of high efficiency dye-sensitized solar cells, Journal of Physical Chemistry B 110 (2006) 25210–25221.
[43] C. Richter, C.A. Schmuttenmaer, Exciton-like trap states limit electron mobility in TiO_2 nanotubes, Nature Nanotechnology 5 (2010) 769–772.